Biocatalytic Asymmetric Alkene Reduction: Crystal Structure and Characterization of a Double Bond Reductase from *Nicotiana tabacum*
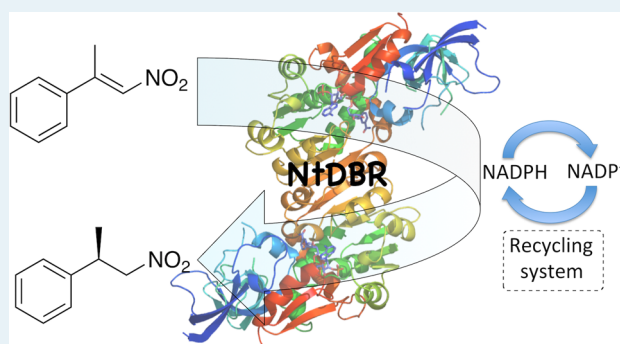
David J. Mansell,[†,⊥,§] Helen S. Toogood,[†,‡,§] John Waller,[†,‡] John M. X. Hughes,[†,‡] Colin W. Levy,[†,‡] John M. Gardiner,[†,⊥] and Nigel S. Scrutton*[,†,‡]

[†]Manchester Institute of Biotechnology, [⊥]School of Chemistry, and [‡]Faculty of Life Sciences, University of Manchester, Manchester, U.K.

Ⓢ *Supporting Information*

ABSTRACT: The application of biocatalysis for the asymmetric reduction of activated C=C is a powerful tool for the manufacture of high-value chemical commodities. The biocatalytic potential of "-ene" reductases from the Old Yellow Enzyme (OYE) family of oxidoreductases is well-known; however, the specificity of these enzymes toward mainly small molecule substrates has highlighted the need to discover "-ene" reductases from different enzymatic classes to broaden industrial applicability. Here, we describe the characterization of a flavin-free double bond reductase from *Nicotiana tabacum* (NtDBR), which belongs to the leukotriene B$_4$ dehydrogenase (LTD) subfamily of the zinc-independent, medium chain dehydrogenase/reductase superfamily of enzymes. Using steady-state kinetics and biotransformation reactions, we have demonstrated the regio- and stereospecificity of NtDBR against a variety of α,β-unsaturated activated alkenes. In addition to catalyzing the reduction of typical LTD substrates and several classical OYE-like substrates, NtDBR also exhibited complementary activity by reducing non-OYE substrates (i.e., reducing the exocyclic C=C double bond of (R)-pulegone) and in some cases showing an opposite stereopreference in comparison with the OYE family member pentaerythritol tetranitrate (PETN) reductase. This serves to augment classical OYE "-ene" reductase activity and, coupled with its aerobic stability, emphasizes the potential industrial value of NtDBR. Furthermore, we also report the X-ray crystal structures of the holo-, binary NADP(H)-bound, and ternary [NADP$^+$ and 4-hydroxy-3-methoxycinnamaldehyde (**9a**)-bound] NtDBR complexes. These will underpin structure-driven site-saturated mutagenesis studies aimed at enhancing the reactivity, stereochemistry, and specificity of this enzyme.

KEYWORDS: *double bond reductase, asymmetric alkene reduction, biocatalysis, crystal structure, Nicotiana tabacum*

■ INTRODUCTION

The intelligent use of enzymes for the production of high-value fine chemicals, pharmaceuticals, and agrochemical intermediates is at the forefront of the drive toward the use of mild and ecologically sustainable manufacturing techniques.[1] This is largely due to the unmatched chemo-, regio-, and stereospecificity that can be achieved when using enzyme-catalyzed reactions with either whole cell preparations or purified enzymes.[1c,2] The biocatalytic asymmetric reduction of activated C=C bonds has received particular attention because of the potential for production of chiral compounds with up to two new stereogenic centers.[3] Recent work has demonstrated the biocatalytic potential of the Old Yellow Enzyme (OYE; E.C. 1.6.99.1) family of oxidoreductases in the reduction of activated α,β-unsaturated alkenes, including α,β-unsaturated aldehydes, ketones, nitroalkenes, and carboxylic acids.[3,4] These FMN-containing, NAD(P)H-dependent oxidoreductases are an exceptionally versatile group of biocatalysts and offer
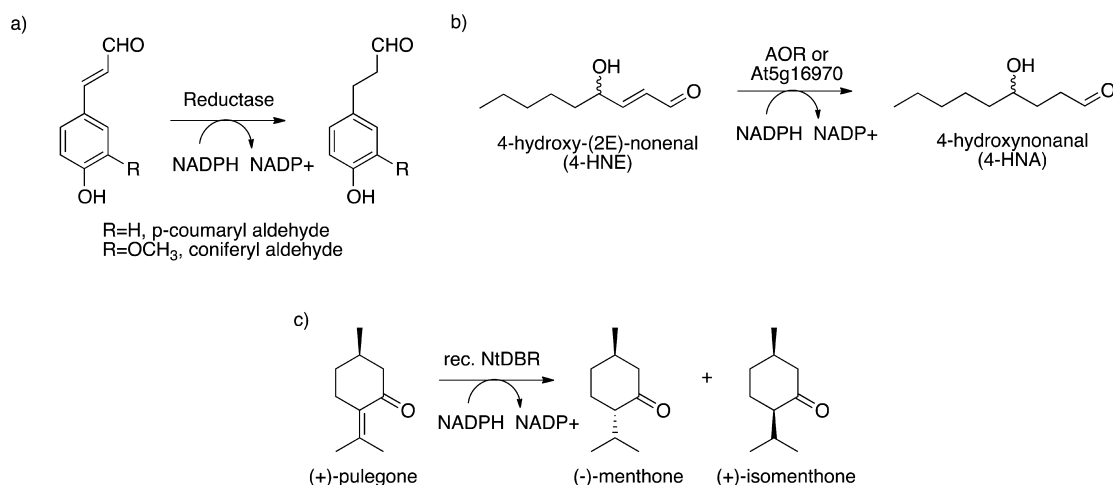
considerable potential for exploitation in industrial biocatalysis; however, the substrate specificity of these enzymes is generally confined to small molecules, which limits the scope of their applicability. This highlights the importance of targeting "-ene" reductases from different enzymatic classes, which could potentially reduce alkene substrates that are not acted upon by OYEs because there is likely to be a significantly altered substrate binding site.

A potential source for "-ene" reductases may exist in the zinc-independent, medium chain dehydrogenase/reductase (MDR) superfamily, or more specifically, the leukotriene B$_4$ dehydrogenase (LTD, MDR002) subfamily.[5] This subclass of enzymes do not contain any bound coenzyme and have been shown to catalyze the reduction of the C=C double bonds of α,β-

Scheme 1. Reactions Catalyzed by the Reductases (a) PtPPDBR and At5g16970, (b) AOR or At5g16970, and (c) NtDBR.[6−9]

a)
R=H, p-coumaryl aldehyde
R=OCH₃, coniferyl aldehyde

b)
4-hydroxy-(2E)-nonenal (4-HNE) → 4-hydroxynonanal (4-HNA)

c)
(+)-pulegone → (-)-menthone + (+)-isomenthone

unsaturated aldehydes, ketones, and carboxylic acids.[6] For example, phenylpropenal double bond reductase (PtPPDBR) from *Pinus taeda* catalyzes the NADPH-dependent reduction of the α,β-unsaturated bond of phenylpropenal aldehydes (Scheme 1a).[7] A similar alkenal double bond reductase (At5g16970) was discovered in *Arabidopsis thaliana*, which reduces the C7−8 alkene group of p-coumaryl- and coniferyl aldehydes (Scheme 1a) and 4-hydroxy-(2E)-nonenal (4-HNE) (Scheme 1b).[6] In rat liver, the detoxification of 4-HNE is catalyzed by the NAD(P)H-dependent alkenal/one oxidoreductase (AOR) to form 4-hydroxynonanal (4-HNA; Scheme 1b).[8] In humans, 4-HNE is a product of lipid peroxidation and can lead to apoptosis, affect cell signaling pathways, and form 4-HNE-protein adducts found in Alzheimer plaques.[6]

A BLAST search of LTD subfamily members identified a putative double bond reductase from *Nicotiana tabacum* (NtDBR). This enzyme has a high amino acid sequence identity to other LTD members: At5g16970 (71%),[6] 2-alkenal reductase (Dbr1) from *Artemisia annua* (67%),[10] (+)-pulegone reductase (PulR) from *Mentha piperita* (66%),[11] and PPDBR (41%).[7] This enzyme was originally misclassified as an NAD⁺-dependent allyl-alcohol dehydrogenase (NtADH) because the enzyme isolated from tobacco leaves showed alcohol dehydrogenase (ADH) activity toward carveol.[12] However, this activity was absent in the recombinant form of the enzyme and purported to be due to the absence of suitable post-translational modification capabilities of the host *Escherichia coli*.[9] NtDBR was later described as a pulegone reductase because of its ability to hydrogenate the exocyclic C=C bond of (R)- and (S)-pulegone to produce menthone and isomenthone isomers (Scheme 1c).[13] In light of the moderate yields achieved for the latter conversion, we have chosen to refer to the enzyme as a generalized double bond reductase (NtDBR). Because menthone and isomenthone have important industrial applications in the production of synthetic peppermint oils and bases, we decided to further investigate the biocatalytic potential of recombinant NtDBR. This paper describes our kinetic characterization of the substrate and cofactor specificity of NtDBR and determination of its regio- and stereospecificity toward typical LTD alkenal/one substrates and commercially useful compounds. We also determined the crystal structure of NtDBR both in isolation (holo) and in complexes with NADP(H) (binary) ± alkene substrate 4-hydroxy-3-methoxycinnamaldehyde (HMCA) (ternary). This

enables us to expand our understanding of the catalytic mechanism and substrate binding modes and drive future structure-driven site-saturated mutagenesis studies to further expand the biocatalytic potential of this enzyme.
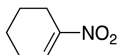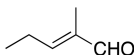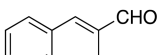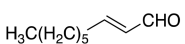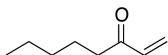
■ EXPERIMENTAL SECTION

Gene Synthesis and Cloning. The protein sequence for the allyl alcohol dehydrogenase (accession number: Q9SLN8) from *N. tabacum* was obtained from UniProt (http://www.uniprot.org). The gene sequence was designed and synthesized by GenScript (USA), incorporating codon optimization techniques of rare codon removal for optimal expression in *E. coli*. The gene was cloned into pET21b (Novagen) via *Nde*I/*Xho*I restriction sites, without a stop codon, to incorporate a C-terminal His₆-tag. The construct was transformed into the *E. coli* strain BL21(DE3)pLysS (Stratagene) for soluble protein overexpression according to the manufacturer's protocol.

Enzyme Production and Purification. The NtDBR construct was grown in Terrific broth medium (ForMedium) containing glycerol (0.4%), ampicillin (100 μg mL^{-1}), and chloramphenicol (34 μg mL^{-1}). Cultures were incubated at 37 °C until OD$_{600\ nm}$ reached 0.5, followed by a 16 h induction with isopropyl-β-D-1-thiogalactopyranoside (IPTG; 10 μM) at 30 °C. Cells were harvested by centrifugation at 5000g for 10 min at 4 °C. Cell pellets were resuspended in lysis buffer (50 mM Tris, pH 8.0) containing the EDTA-free complete protease inhibitor cocktail (Roche), DNase I (0.1 mg mL^{-1}), and lysozyme (1 mg mL^{-1}) and stirred for 20 min at 4 °C. Cells were disrupted by sonication (Sonics Vibra Cell), followed by extract clarification by centrifugation for 60 min at 26 600g.

The supernatant was filtered (0.2 μm) and applied to a Ni²⁺ Sepharose high-performance column (40 mL; GE Healthcare) preequilibrated in buffer A (50 mM Tris, pH 8.0, containing 300 mM NaCl, 10 mM imidazole, and 10% glycerol). The column was washed with five column volumes of buffer A, followed by a step elution of NtDBR into buffer B (50 mM Tris, pH 8.0, containing 300 mM NaCl, 300 mM imidazole, and 10% glycerol). The enzyme was dialyzed against buffer C (50 mM Tris, pH 8.0, containing 10% glycerol) and reapplied to the Ni²⁺ Sepharose column, preequilibrated as before. The column was washed as above, and the enzyme was eluted in a linear gradient (300 mL) to buffer D (50 mM Tris, pH 8.0, containing 300 mM NaCl, 500 mM imidazole, and 10% glycerol). The enzyme was dialyzed against buffer C as above,

Table 1. Steady-State Kinetic Parameters of NtDBR with a Variety of Substrates[a]

Substrate	Structure	pH 5.4			pH 7.3		
		App. k_{cat} (s^{-1})	App. K_m (μM)	k_{cat}/K_m (s^{-1}mM^{-1})	App. k_{cat} (s^{-1})	App. K_m (μM)	k_{cat}/K_m (s^{-1}mM^{-1})
NADPH	-	-	5.8±0.6[1]	ND	(1.3±0.03)[1]	ND	ND
1a		>11[2]	>400[2]	16	1.46±0.02	57±3	25.6
2a		9.2±1.6	1032±211	8.9	0.66±0.01	837±51	0.8
3a		>3.5[2]	>1000[2]	2.8	1.10±0.02	516±21	2.1
4a		(2.92±0.08)	ND	ND	(0.87±0.07)	ND	ND
5a		(1.17±0.05)	ND	ND	(0.52±0.03)	ND	ND

[a]Standard reactions were performed in 50 mM K$_2$HPO$_4$/KH$_2$PO$_4$ pH 7.3 + 1 mM alkene, 5% ethanol and 100 μM NADPH. Data in parentheses are the rates (s^{-1}) with 1 mM alkene rather than k_{cat}. ND = not determined. Alkenes not reduced by NtDBR under steady-state conditions were methyl α-methyl-*trans*-cinnamate, methyl *trans*-cinnamate, *trans*-cinnamonitrile, *trans*-cinnamic acid, *trans*-4-phenyl-3-buten-2-one, 2-cyclohexenone, 3-methyl-2-cyclohexen-1-one, 1-cyclohexene-1-carboxylic acid, 1-cyclohexene-1-carbonitrile, 2-cyclohexen-1-ol, 2-cyclopenten-1-one, 2-methyl-2-cyclopenten-1-one, 3-methyl-2-cyclopenten-1-one, 3-methyl-2-butenal, citral, (5*R*)- and (5*S*)-carvone, ketoisophorone, isophorone, 2-methylmaleimide, *N*-phenyl-2-methylmaleimide, itaconic acid, mesaconic acid, citraconic acid, crotonitrile, (*S*)-perillyl alcohol, and β-bromostyrene. [1]Reactions were performed in the presence of 500 μM nitrocyclohexene, which is below the expected K_m for this substrate. [2]Estimated kinetic parameters are based on fits of partial Michaelis−Menten plots due to substrate concentration range limitations.

concentrated by ultrafiltration, and flash frozen in liquid nitrogen for storage at −80 °C. Purity was assessed by SDS−PAGE, and the concentration was determined using the Bradford and extinction coefficient methods ($ε_{205}$ = 30.86 mg mL^{-1}).[14]

Crystallogenesis and Data Collection. Crystals of the C-terminally His$_6$-tagged NtDBR were obtained by sitting drop vapor diffusion at 20 °C after a period of 7 days of incubation. Drops were prepared by mixing equal volumes (2 μL) of mother liquor (100 mM KH$_2$PO$_4$/citrate buffer, pH 4.0−5.0, containing PEG 300 (35−50%)) and NtDBR (25 mg mL^{-1} in 10 mM Tris, pH 7.0). Crystals of the holoenzyme were flash-frozen in liquid nitrogen in the absence of any additional cryoprotectant. Additional crystals were soaked in mother liquor containing (A) NADPH or (B) NADP$^+$ and 4-hydroxy-3-methoxycinnamaldehyde to form the binary and ternary complexes, respectively. All ligand concentrations were at half saturation, and crystals were flash frozen in liquid nitrogen in the absence of any additional cryoprotectant. Full holo-NtDBR (1.94 Å), binary-NtDBR (1.9 Å), and ternary-NtDBR (2.1 Å) X-ray diffraction data sets were collected from single crystals at the Diamond Light Source (Oxford, UK).

Structure Determination and Refinement. Data were processed and scaled using the programs MOSFLM[15] and Scala.[16] The structures were solved via molecular replacement using the program MolRep[16] and the coordinates for a Swiss-MODEL-generated pdb file of NtDBR (http://swissmodel.expasy.org). This model was generated on the basis of the known three-dimensional structure of *Arabidopsis* alkenal double bond reductase At5g16970 (PDB 2J3H).[6] Positional, TLS (two domains per monomer), and isotropic B-factor refinement was performed using REFMAC5,[17] with alternate rounds of manual rebuilding of the model and water addition in COOT.[16] Data and refinement statistics are shown in Table 2. The atomic coordinates and structure factors (codes: 4HFJ, 4HFM and 4HFN, for the holo, binary, and ternary structures, respectively) have been deposited in the Protein Data Bank,

Research Collaboratory for Structural Bioinformatics, Rutgers University, New Brunswick, NJ (http://www.rcsb.org/). The interactions involved in the dimeric interfaces were analyzed by the protein interfaces, surfaces, and assemblies service PISA at the European Bioinformatics Institute (http://www.ebi.ac.uk/msdsrv/prot_int/pistart.html).[18]

Steady-State Kinetics. Steady-state kinetic analysis was performed on a Cary UV-50 Bio UV/vis scanning spectrophotometer using a quartz cuvette (1 mL; Hellma) with a 1 cm path length. Reactions (1 mL) were performed in buffer (50 mM Tris, pH 7.4) containing NADPH (0.1 mM), alkene (1 mM added as concentrated stocks in ethanol to a final concentration of 5%) and enzyme (10 nM−4 μM). Reactions were followed continuously by monitoring NADPH oxidation at 340 nm ($ε_{340}$ = 6220 M^{-1} cm^{-1}) for 1 min at 25 °C. Reactions with alkenes that absorb at 340 nm were monitored at 365 nm ($ε_{365}$ = 3256 M^{-1} cm^{-1}). Standard units of activity (1 μmol NADPH min^{-1} mg^{-1} NtDBR after protein purification) were determined in buffer (50 mM KH$_2$PO$_4$/K$_2$HPO$_4$, pH 5.4) containing 100 μM NADPH and 500 μM 1-nitrocyclohexene at 25 °C. Typical batches contained 2.01−2.47 U/mg enzyme. All comparative reactions were performed using the same enzyme batch. To determine the optimal reaction conditions and steady-state reaction parameters (k_{cat}, K_m, and K_i), the reaction pH (5.0−7.4), buffer (KH$_2$PO$_4$/K$_2$HPO$_4$ or KH$_2$PO$_4$/K$_2$HPO$_4$/citrate), enzyme (10 nM−4 μM), and substrate concentrations (10 μM−10 mM) were varied. In cases that reaction constraints prevented a full steady-state analysis, the specificity factor (k_{cat}/K_m) was determined from the initial Michaelis−Menten slope. Substrate concentrations were mostly determined using their respective extinction coefficients previously described,[19] or as follows: *trans*-2-nonenal ($ε_{227}$ = 15 600 M^{-1} cm^{-1}), 1-octen-3-one ($ε_{214}$ = 8500 M^{-1} cm^{-1}), methyl crotonate ($ε_{210}$ = 12 500 M^{-1} cm^{-1}), (*R*)-pulegone ($ε_{263}$ = 6310 M^{-1}cm^{-1}).

Biotransformation with NtDBR. All reagents were of analytical grade. The alkenes were dissolved as stock solutions

Table 2. X-ray Crystallographic Data Collection and Refinement Statistics[a]

parameters[b]	holo NtDBR	binary NtDBR	ternary NtDBR
space group	C2	C2	C2
cell dimensions			
a, b, c (Å)	88.57, 148.74, 67.73	88.20, 149.84, 66.61	88.86, 149.86, 66.21
α, β, γ (°)	90.0, 115.59, 90.0	90.0, 115.53, 90.0	90.0, 115.96, 90.0
resolution (Å)	42.13−2.00 (1.99−2.00)	60.1−1.9 (2.00−1.90)	37.47−2.01 (2.06−2.01)
R_{merge} (%)[c]	5.5 (66.4)	8.8 (36.8)	7.2 (45.9)
$I/\sigma I$	15.5 (2.3)	11.7 (3.6)	9.4 (2.3)
completeness (%)	98.8 (98.0)	97.8 (95.2)	98.1 (99.3)
redundancy	4.8 (4.8)	5.8 (4.3)	3.2 (3.2)
no. reflections	275 755	346 704	161 936
unique reflections	57 956	59 835	51 397
R_{work}/R_{free}	18.2/22.7 (25.0/28.6)	17.3/20.6 (21.8/25.8)	17.2/22.1 (22.2/27.3)
RMS deviations			
bond angles (°)	1.541	1.612	1.769
bond lengths (Å)	0.018	0.016	0.020
Ramachandran plot			
allowed region (%)	97.0	98.3	97.3
additionally allowed region (%)	2.7	1.7	2.7

[a]PDB codes for Holo-NtDBR, binary-NtDBR and ternary-NtDBR are 4HFJ, 4HFM, and 4HFN, respectively. [b]Highest resolution shell is shown in parentheses. [c]$R_{merge} = \Sigma_{hkl} \Sigma_i |I_i(hkl) - [I(hkl)]|/\Sigma_{hkl} \Sigma_i I_i(hkl)$, where $I_i(hkl)$ is the intensity of the ith observation of unique reflection hkl. Redundancy = total number of reflections/total unique reflections. $R_{work} = \Sigma||F_{obs}| - |F_{calc}||/\Sigma|F_{obs}|$, where F_{obs} and F_{calc} are observed and model structure factors, respectively. R_{free} was calculated by using a randomly selected set (5%) of reflections.

in ethanol, then diluted to 5 mM in the reactions (2% final solvent concentration). (i) *Standard biotransformations:* Standard reactions (1.0 mL) were performed aerobically in phosphate buffer (50 mM KH_2PO_4/K_2HPO_4 pH 6.4) containing alkene (5 mM), NtDBR (2.0 μM), NADP⁺ (10 μM), glucose (15 mM), and glucose dehydrogenase (GDH; 10 U). The reactions were shaken at 30 °C for 4 or 24 h at 130 rpm, and terminated by extraction with ethyl acetate (0.9 mL) containing an internal standard. The extracts were dried using anhydrous $MgSO_4$ and analyzed by GC to determine the percent yield, percent conversion, and enantiomeric excess. Products were identified by comparison with authentic standards. (ii) *Effect of pH:* Reactions were performed as described for the standard biotransformations, except a variety of buffer compositions and final pH values were used (50 mM KH_2PO_4/K_2HPO_4, pH 6.0−7.4; or 50 mM KH_2PO_4/K_2HPO_4/citrate, pH 5.4−6.0). (iii) *Reduction of (5R)-pulegone in the presence of auxiliaries:* Reactions (1.0 mL) were performed as described under the standard biotransformations conditions with the addition of Triton X-100 (0.01% or 0.1%) ± BSA (15 μM) or in the presence of BSA (15 μM) alone. (iv) *Biotransformations with PETN reductase:* PETN reductase was produced and purified as described previously.[20] Reactions (1.0 mL) were performed anaerobically in buffer (50 mM KH_2PO_4/K_2HPO_4 pH 7.0) containing PETN reductase (2.0 μM). Reactions were set up within an anaerobic glovebox (Belle Technology Ltd.) under a nitrogen atmosphere (<5 ppm oxygen) using anaerobic solvents. Prior to addition, PETN reductase was deoxygenated by passage through a BioRad 10DG column equilibrated in anaerobic reaction buffer. All other details were the same as those described under the standard biotransformation conditions.

■ RESULTS AND DISCUSSION

Substrate Specificity of NtDBR. The activity of NtDBR toward a variety of activated alkenes was determined under steady-state conditions (Table 1). Surprisingly, the pH optimum was found to be 5.4 with 1-nitrocyclohexene (**1a**) (Supporting Information Figure S1), in contrast to prior reported reaction conditions of pH 7−8.[9,12,13] Given that typical biotransformation reactions proceed around neutral pH, we determined the steady-state kinetic parameters of NtDBR at both pH 5.4 and 7.3 (Table 1). In many cases, full steady-state kinetic parameters could not be determined because of either limited alkene solubility (*trans*-2-nonenal, **4a**), significant alkene absorbance at 340/365 nm at higher substrate concentrations [**1a** and *trans*-cinnamaldehyde (**6a**)], or the detection of near-zero-order kinetics with respect to substrate concentration down to 10−20 μM [1-octen-3-one (**5a**) and NADPH at pH 7.3]. In these cases, either the specificity factor (k_{cat}/K_m) or the rate with 1 mM alkene was determined (Table 1).

NtDBR showed a higher preference for NADPH as the hydride donor[13] compared with NADH (>1600-fold). This is not surprising, given the significant number of specific interactions observed between the enzyme and the adenosyl phosphate group in the binary and tertiary structures (vide infra: Structural Analysis of NtDBR) (Figure 2B). This preference for NADPH was also seen with Dbr1[10] and rat AOR[21] and may be a common feature of LTD enzymes. Although full steady-state parameters could not be determined for some substrates, NtDBR shows a high preference for 1-nitrocyclohexene (**1a**) over typical LTD alkenal/one substrates (Table 1). However, significant activity was detected with alkenals: 2-methylpentenal (**2a**) and *trans*-cinnamaldehyde (**6a**) at pH 5.4 (k_{cat}/K_m = 8.9 and 2.8, respectively), although the K_m is predicted to be higher (millimolar range) than with **1a**. In contrast, the K_m values with AOR-like substrates *trans*-2-nonenal (**4a**) and 1-octen-3-one (**5a**) are predicted to be in the low micromolar range, similar to NADPH binding (results not shown). They showed reaction rates (0.87 ± 0.07 and 0.52 ± 0.03 s⁻¹, respectively) similar to **2a** and **6a** (0.36 ± 0.02 and 0.80 ± 0.03 s⁻¹, respectively) at pH 7.3. In addition, substrate
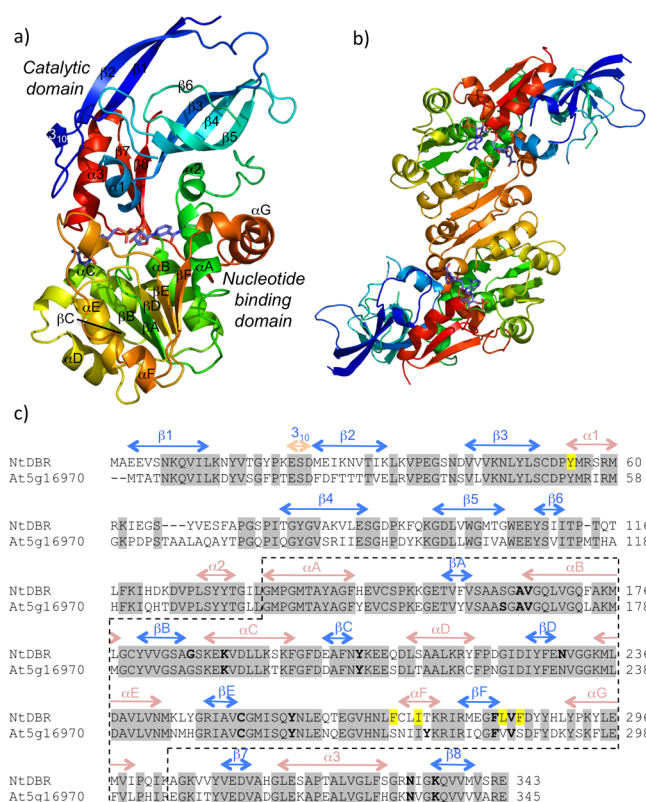
inhibition was seen with **2a** (apparent K_i = 2.6 ± 0.6 mM) and **5a**, although only at pH 5.4.

NtDBR is predicted to display tight binding with **4a** and **5a** (zero-order kinetics down to 10 μM substrate; results not shown); therefore, it is likely to be specific for long chain fatty alkenals/ones. LTD family members commonly reduce the substrate **4a**, displaying tight binding kinetics, high rates, or both. For example, At5g16970 showed both a high catalytic rate (k_{cat} = 51 s^{-1}) and apparent tight binding (K_m = 5.9 μM) toward **4a**.[22] In contrast, enzymes Dbr1 and AOR showed apparent tight binding (K_m = 6.4/77.6 μM), but slower reaction rates (k_{cat} = <1/0.2 s^{-1}) with **4a**.[10,21]

A comparison of the kinetic parameters of NtDBR at pH 5.4 vs 7.3 shows an interesting trend of a decrease in both the catalytic rate and K_m with increasing pH (Table 1). This trend could possibly be due to a change in the position of the substrates α,β-unsaturated bond relative to the NADPH *pro-4R* hydrogen at neutral pH, resulting in a tighter-binding, yet less favored enzyme−substrate complex. Alternatively, the change in the overall rate may be due to a decrease in the product(s) K_D, dissociation rates, or both. Further, fast reaction kinetics studies are required to determine the mechanism of the pH effects on the overall reaction kinetics.

Minor activity (<0.1 s^{-1}) was seen under standard steady-state conditions with alkene substrates: α-methyl *trans*-cinnamaldehyde, 1-cyclohexene-1-carboxaldehyde, methyl crotonate, (*R*)-pulegone, and dimethyl itaconate. No reduction was seen with other activated alkenes, such as maleimides, citral, (5*R*)- or (5*S*)-carvone, (*S*)-perillyl alcohol, and substituted cyclohexenones and cyclopentenones (see Table 1 footnote for full list). The poor reactivity with (*R*)-pulegone was unexpected, given the detection of significant activity in prior studies by others (k_{cat} = 3.3 s^{-1}, K_m = 1.4 mM);[9] however, the earlier studies were carried out under biotransformation conditions (pH 7.0, 3 mM NADPH, 1 mM dithiothreitol, 0.2% Triton X-100), and the presence of Triton-X-100 is known to dramatically enhance the catalytic rate of NtDBR.[13] In addition, previous comparative studies of alkene reduction by pentaerythritol tetranitrate reductase and thermostable Old Yellow Enzyme (TOYE) showed that significant alkane product could be detected in biotransformations with substrates poorly reduced under steady-state conditions.[19a,23] Therefore, longer biotransformation reactions (24 h; 5 mM alkene) allow a more comprehensive investigation of the substrate range of alkene reduction.

Structure Analysis of NtDBR. We determined the X-ray crystal structures of the holo-, binary (NADP(H)-bound), and ternary (NADP$^+$ and 4-hydroxy-3-methoxycinnamaldehyde-bound) NtDBR complexes. The data collection and refinement statistics can be found in Table 2. The asymmetric unit of each structure contains two protein molecules, related by a noncrystallographic 2-fold axis (C_2 symmetry). The overall structure of NtDBR exhibits a typical MDR-like protein fold (Figure 1A), arranged as a functional homodimer (Figure 1B).[24] Each monomer is composed of two domains (Figure 1A): a substrate binding or catalytic domain (residues 1−135 and 304−343) and a nucleotide-binding domain (residues 136−303). The catalytic domain contains three α-helices and eight β-strands, with the majority of the β-strands forming a twisted partial β-barrel-like structure, as seen in At5g16970 structures (Figure 1C).[6] In contrast, the nucleotide-binding domain contains a typical alternating pattern of α-helices (αA-αG) and β-strands (βA-βF), forming a Rossman fold seen in
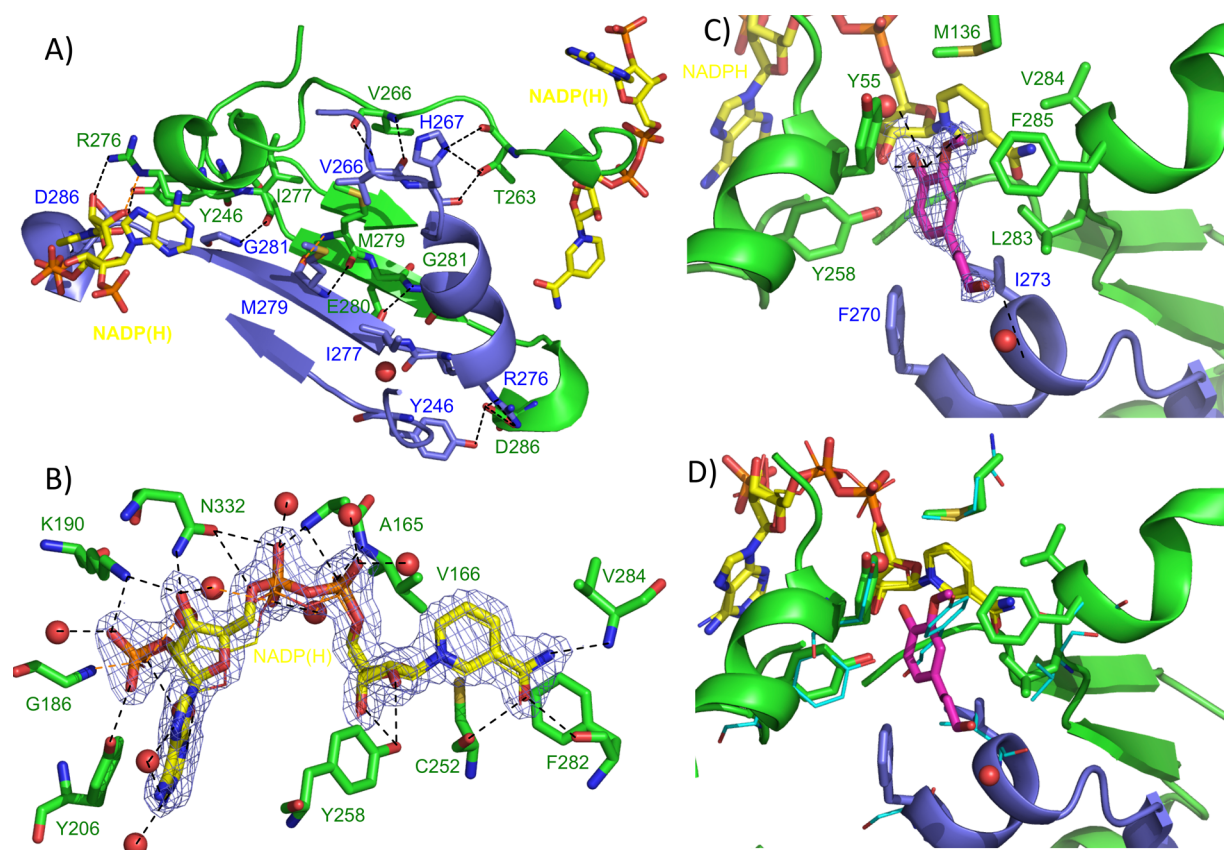

Figure 1. The overall structure of NADP(H)-bound NtDBR (a) monomer and (b) dimer. Each structure is shown as a cartoon with a gradient from blue at the N-terminus to red at the C-terminus. The secondary structure elements are labeled in part a, including indicating where β6 is present in other structures. NADP(H) is shown as atom colored sticks with blue carbons. (c) ClustalW alignment of the protein sequences of NtDBR and At5g16970 double bond reductases. The α-helices and β-sheets are indicated as red and blue bars/labels, respectively. The dotted box highlights the residues making up the nucleotide-binding domain. Residues highlighted in bold text are involved in NADP(H)-binding. Residues highlighted with yellow shading are within van der Waals distance to 4-hydroxy-3-methoxycinnamaldehyde in the ternary complex.

many nucleotide-binding enzyme structures. The active site is formed in a groove located at the interface of the two domains, with a minor contribution of residues from the neighboring monomer.

Using the program DALILITE,[25] each of the three structures was shown to be virtually identical (rmsd of 0.5−1.0 Å) with Z scores of 49.6−54.5 (331 residues aligned by Cα). NtDBR is also very similar to the structure of another LTD subfamily member At5g16970 (rmsd of 0.8−1.1 Å; Z score = 47.4−50.8).[6] Further details of the subtle differences among the three NtDBR structures and At5g16970 can be found in the Supporting Information.

Dimeric Interface. The dimeric interface is composed of residues located in the nucleotide-binding region (αE-βF) of each subunit (Figure 1C; Supporting Information Table 2). These secondary structure elements are oriented antiparallel with respect to each monomer chain, particularly in the case of strand βF (Figure 1A and 2B). This gives the appearance of an extended β-sheet across the dimer interface, similar to the At5g16970 structure.[6] An analysis of the dimeric interface of each structure gave complex formation significance scores (CSS) of 0.5−1.0, with interface areas of 1019−1058 Å^2. This is

Figure 2. (A) Structure of the dimeric interface of NADP(H)-bound NtDBR. (B) NADP(H)-binding mode of the binary NtDBR crystal structure. The omit $|F_o| - |F_c|$ map of NADP(H) in subunit A is shown as a blue mesh. (C) Crystal structure of the active site of the NADP$^+$- and HMCA-bound NtDBR crystal structure. The omit $|F_o| - |F_c|$ map of HMCA is shown as a blue mesh. (D) Superimposition of the alkene/alkane binding pockets in the ternary structures of NtDBR and At5g16970 (pdb: 2J3J and 2J3F). Residues surrounding the HMCA binding site are shown as atom colored sticks with green and blue carbons for subunits A and B, respectively. NADP$^+$ and HMCA/4-HNE are shown as atom-colored sticks with yellow and teal/orange carbons, respectively. Residue numbers are color-coded according to the enzyme residue carbon color. In each part, the protein is shown as green and teal cartoons or sticks, for subunits A and B, respectively. NADP(H) is shown as atom colored sticks with yellow carbons. Water molecules are shown as red spheres. Interactions are shown as dotted lines (orange lines refer to interactions occurring behind the atoms shown).

indicative of a functional interaction,[18] consistent with the observation that wild-type and recombinant NtDBR exist as a homodimer in vitro.[9,12]

The interactions within the dimeric interface are composed of mainly hydrogen bonds between backbone (e.g., G281 N−I277 O) or side chain atoms (e.g., H267 ND1−263 OG1; Supporting Information Table 1). In some cases, pairs of the same residues of each subunit interact via backbone N and O atoms (V266 and M279). Salt bridges also play a role in the interface, with multiple interactions seen between residues R276 and D286 of each subunit (Supporting Information Table 1). Residues E280 (OE2) and R276 (O) of subunits A and B, respectively, also interact via the presence of a bridging water molecule. Interestingly, the βF region (residues 277−286) in LTD enzymes is known to be involved in NADP(H) binding (Figure 2A),[6] suggesting the dimeric state may be important for either substrate binding, enzyme activity, or both.

NADP(H)-Binding Site. Both the binary and ternary crystal structures showed clear $|F_o| - |F_c|$ electron density for the NADP(H) (Figure 2B). The cofactor binds in the cleft joining the catalytic and nucleotide-binding domains in an extended conformation (Figure 1), similar to other LTD enzymes. In the holoenzyme, this cleft is filled with water molecules, and the backbone positions of surface regions α1 and β7-α3

surrounding the NADP(H) binding site are slightly altered in position compared with the binary and ternary structures. The side chain positions of residues Y206, N332, and S136 are significantly different between the holoenzyme and the NADP(H)-bound structures. In the case of S136, this is to prevent a clash of this residue with the nicotinamide moiety of NADP(H).

The position and orientation of NADP(H) in subunit A of the binary and ternary structures are virtually identical. In contrast, the mode of NADP(H) binding in subunit B of the binary complex differs significantly because of a reorienting of atoms O5B and C5B of the adenosine moiety (Figure 2B). The position of the nicotinamide moiety in these structures and the At5g16970 binary and ternary complexes is highly conserved;[6] however, the orientation of the remaining cofactor atoms can vary significantly between subunits and between enzymes. In the case of the At5g16970 ternary complex, the cofactor reorients beginning at the D-ribose moiety relative to NtDBR, although the positions of the terminal adenine base and phosphate group are similar in both structures.[6] Further details about the more subtle differences in the NADP(H) binding can be found in the Supporting Information.

Ternary Complex. The crystal structure of NtDBR in the presence of the alkene substrate derivative 4-hydroxy-3-

methoxycinnamaldehyde (HMCA) and product NADP$^+$ showed clear $|F_o| - |F_c|$ electron density for the presence of NADP$^+$ and a second ligand in subunit A only (Figure 2C, D); however, the electron density for the putative propenal ring substituent of HMCA was partially disordered and nonplanar with respect to the aromatic ring. The close proximity of the side chain of L283 to the propenal group of HMCA may be causing it to be oriented in a less favored nonplanar conformation. Alternatively, the second ligand could potentially be the alkane product derivative 4-hydroxy-3-methoxyhydro-cinnamaldehyde (HMHCA), with substrate hydrogenation occurring via X-ray exposure during data collection. Therefore, we are unable to ascertain the exact nature of the second ligand and have modeled in HMCA because this was the compound soaked into the crystals.
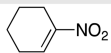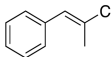
Unfortunately, we cannot directly infer the likely active binding mode of HMCA because the substrate/product is bound in an orientation with the propanal group at the protein surface, distal from the NADP$^+$ nicotinamide moiety (Figure 2C). Therefore, the ternary complex is likely an inhibitory complex, although the position of HMHCA aids us in determining which residues are likely to be involved in forming the alkene substrate binding pocket. In contrast to NADP(H) binding, there are no hydrogen bonds between HMHCA and the protein. This is consistent with the observation that there is little change in the position of residues lining the alkene-binding pocket between the structures, with the exception of mobile surface residues F285 and E29. Instead, there are direct polar interactions between the 4-OH group (O11) of HMHCA and both the N1N and O2D atoms of NADP$^+$ (Figure 2C; Supporting Information Table 3). These interactions are likely responsible for the orientation of HMHCA in an inhibitory complex. The binding pocket contains six hydrophobic residues within van der Waals distance of HMHCA, including two conserved NADP(H)-binding residues (Y55 and Y258), and two nonconserved residues from subunit B (F270 and I273).

A superimposition of the ternary structures of NtDBR and At5g16970 (NADP$^+$ and *p*-coumaryl aldehyde (PCA) or 4-HNE) showed significant differences in the second ligand binding positions (Figure 2D). This is due to the binding of PCA and 4-HNE in a likely active conformation to At5g16970. A comparison of the residues lining the alkene-binding site in both structures shows a high conservation in sequence identity and residue position in most cases. Notable exceptions include two phenylalanine-to-serine substitutions (NtDBR to At5g16970; 285/287 and 270/272), which effectively introduce additional polar residues into the latter enzyme. In the case of F285, this residue clashes with PCA and would likely have to reorient to allow the binding of cinnamaldehyde-like substrates in an active conformation. Therefore, the presence of two additional phenylalanine residues may restrict the size of the binding pocket and impact on the enzyme substrate specificity. Further site-directed mutagenesis work is required to confirm the mechanistic role(s) of individual residues in substrate binding and catalysis and confirm whether the dimeric form is required for catalysis.

Biotransformations with NtDBR. To fully evaluate the biocatalytic potential of NtDBR and gain an insight into the stereochemical outcome of these reactions, we studied the reduction of a variety of compounds with different activating groups and substitution patterns under biotransformation conditions. Under steady-state conditions, a decrease in both the catalytic rate and K_m was observed with increasing pH

(Table 1); therefore, we studied the overall effect of pH on the NtDBR-catalyzed reduction under biotransformation conditions. In addition, changes in pH have also been shown to influence the enantiopurity of products that are subject to racemization under the reaction conditions.[19a] The assays were performed aerobically against two representative substrates, 1-nitrocyclohexene (**1a**) and methyl-*trans*-2-methylcinnamalde-hyde (**3a**) (5 mM substrate; 2 μM NtDBR), for 4 and 24 h at pH 5.4, 6.4, and 7.4 using a NADP$^+$/glucose dehydrogenase (GDH) cofactor recycling system as the source of reducing equivalents (Table 3).

Table 3. Influence of pH on the Reduction of 1a and 3a by NtDBR^a

Substrate	Structure	Time [h]	pH 5.4		pH 6.4		pH 7.4	
			Conv. [%]	Yield [%]	Conv. [%]	Yield [%]	Conv. [%]	Yield [%]
1a	⬡—NO₂	4	100	95	100	95	37	7
		24	-	-	-	-	86	9
3a	⬡—CHO	4	55	61	89	87	90	88
		24	83	65	100	88	100	89

^{a}Conditions: reactions (1 mL) were performed aerobically in buffer (50 mM KH₂PO₄/K₂HPO₄, pH 7.4 and 6.4; or 50 mM KH₂PO₄/K₂HPO₄/citrate, pH 5.4) containing alkene (5 mM), NtDBR (2 μM), NADP$^+$ (10 μM), glucose (15 mM) and glucose dehydrogenase (GDH; 10 U). The reactions were agitated at 30 °C for 4 or 24 h at 130 rpm. Conversion (conv) and yields were determined by GC analysis on a DB-WAX column. The alkenes were added from stock solutions in ethanol (2% final solvent concentration in the reactions). The product obtained during the reduction of **3a** was near racemic in all cases.

The reduction of 1-nitrocyclohexene (**1a**) proceeded efficiently at both pH 5.4 and 6.4, with complete conversion of the substrate observed after 4 h; however, at pH 7.4, the reduction was significantly slower and had failed to reach completion after 24 h, consistent with the rates observed under steady-state conditions (see above). Furthermore, poor product yields were observed at pH 7.4, despite apparent high substrate consumption, indicating decomposition of substrate, product, or both. In contrast, the reduction of methyl-*trans*-cinnamalde-hyde (**3a**) was most efficient at pH 6.4 and 7.4, with almost identical results obtained at both pH values. Changes in pH did not influence the stereochemical outcome, as near-racemic product was obtained at all pH values. Therefore, the optimum pH for reduction was considered to be pH 6.4, and all further assays were performed at this pH.

NtDBR proved to be highly efficient in the reduction of several typical LTD-like substrates: 2-methylpentenal (**2a**), 1-octen-3-one (**5a**), and *trans*-cinnamaldehyde (**6a**), all of which were completely reduced after 4 h (Table 4). In contrast, 1-cyclohexene-1-carboxaldehyde (**7a**) and citral (**8a**) were reduced with moderate and low yields, respectively. In terms of stereoselectivity, the reduction of citral **8a** [the citral used here was a mixture of geranial (*E*)-**8a** and neral (*Z*)-**8a** in ~65:35 ratio] is complicated by isomerization of this substrate between its *E/Z* forms under the reaction conditions.[19a] Some reduction of 4-hydroxy-3-methoxycinnamaldehyde (**9a**) was observed, despite the apparent inhibitory binding conformation observed in the tertiary crystal structure (Figure 2C). This suggests that more than one binding conformations may exist for this ligand.

Table 4. Reduction of Various Activated Alkenes by NtDBR Using an NADP$^+$/GDH Cofactor Recycling System[a]

Substrate	Product	Time (h)	Conv.[b] (%)	Yield[b] (%)	ee[c] (%)
1a (1-nitrocyclohexene)	1b	4	100	>99	-
2a	(rac)-2b	4	100	96	0
3a	(rac)-3b	4	70	68	0
		24	100	97	0
4a	4b	4	88	72	-
		24	100	>99	-
5a	5b	4	100	87	-
6a	6b	4	100	>99	-
7a	7b	4	53	39	-
		24	84	55	-
8a	(S)-8b	4	18	10	50
		24	58	12	45
9a	9b	4	6[e]	5[e]	-
		24	29[e]	20[e]	-
(E)-10a	(R)-10b	4	69	67	>99
		24	95	93	>99
(Z)-10a	(S)-10b	4	70	69	51
		24	92	81	45
11a	(rac)-11b	4	71	59	0
		24	91	75	0
(5R)-12a	(2R,5R)-12b	4	24	22[d]	10[(de)]
		24	74	61[d]	25[(de)]

[a]Conditions: reactions (1 mL) were performed aerobically in buffer (50 mM KH_2PO_4/K_2HPO_4, pH 6.4) containing alkene (5 mM), NtDBR (2 μM), NADP$^+$ (10 μM), glucose (15 mM), and glucose dehydrogenase (GDH; 10 U). The reactions were agitated at 30 °C for 4 or 24 h at 130 rpm. The alkenes were added from stock solutions in ethanol (2% final solvent concentration in the reactions). [b]Conversion (conv) and yields were determined by GC analysis using a DB-WAX column. [c]By chiral GC. [d]Total yield of diastereoisomers [(2S, 5R)-menthone and (2R, 5R)-isomenthone] [e]By GC analysis using a Rtx-5 ms column. NtDBR did not catalyze the reduction of the following substrates: methyl *trans*-cinnamate, dimethyl itaconate, methyl crotonate, (S)-perillyl alcohol, (5R)- and (5S)-carvone, and 2-methylmaleimide.

The reduction of the *E* and *Z* isomers of 2-phenyl-1-nitroprop-1-ene (**10a**) proceeded with an opposite stereochemical outcome: the reduction of (*E*)-**10a** furnished the *R* product in optically pure form, whereas the reduction of (*Z*)-**10a** generated the *S* product with poor enantioselectivity (Table 4). This is in contrast to our previous observations with the Old Yellow Enzyme, PETN reductase, which furnished the same *S* enantiomer from the reduction of both (*E*)- and (*Z*)-**10a** with moderate and high optical purity, respectively.[19a] In the case of PETN reductase, this was attributed to multiple substrate binding conformations for (*E*)-**10a**, with the preference for the *S* product under anaerobic conditions.[19a,20] Therefore, it is likely that in NtDBR, the *E* and *Z* isomers bind predominantly in the same conformation, leading to an enantiodivergent outcome. The lower ee values obtained from the reduction of (*Z*)-**10a** may originate from isomerization between the *E*/*Z* forms or a second, less favored, binding conformation of the *Z* isomer in the NtDBR active site. Significantly, we are now able to generate both enantiomers of **10b** in optically pure form by using either PETN reductase or NtDBR, eloquently highlighting the potential of this enzyme as a complementary biocatalytic tool to classical OYE "-ene" reductases. The related 1-phenyl-2-nitropropane (**11b**) was also obtained under the reaction conditions, albeit in racemic form. The low enantiopurity of **11b** and other products possessing a stereogenic center at the Cα position (**2**−**3b**) has been attributed to the product racemization in aqueous media.[19a,26] In such circumstances, a biphasic reduction system may be employed to deliver improved product enantiopurity.[27]

Although some differences were seen in the enantioselectivity of the reactions catalyzed by NtDBR vs PETN reductase, the product yields from both reactions were similar with substrates **1a** (both >99%) and **2a** (96 vs 85%). More significant differences in product yields were seen with substrates **8a** (12% vs 56%) and (*E*)-**10a** (93 vs 70%) for DBR and PETN reductase, respectively. The reduction of (*R*)-pulegone (**12a**) afforded (2*S*,5*R*)-menthone and (2*R*,5*R*)-isomenthone (Scheme 1c) in moderate yield and in a ratio of ∼1:2. In contrast, a putative second enzyme present in *N. tabacum* has been shown to catalyze the reduction of (*R*)-**12a** with high yields and stereoselectivity, producing almost entirely (2*R*,5*R*)-isomenthone.[28] Prior studies suggested an improvement in

Table 5. Reduction of Various Activated (R)- and (S)-Perillaldehyde (13a) by NtDBR and PETNR[a]

Substrate	Product	Enzyme	Conf.[b]	Time (h)	Conv. (%)[b]	Yield (%)[b]	cis/trans (%)[b]
(S)-13a	13b	NtDBR	cis	4	96	93	64
			cis	24	100	96	45
		PETNR	trans	4	100	>99	89
			trans	24	100	80	91
(R)-13a		NtDBR	cis	4	63	59	70
			cis	24	100	92	75
		PETNR	cis	4	95	92	95
			cis	24	100	56	60

[a]Conditions: NtDBR reactions (1 mL) were performed aerobically in buffer (50 mM KH_2PO_4/K_2HPO_4, pH 6.4) containing alkene (5 mM), NtDBR (2 μM), $NADP^+$ (10 μM), glucose (15 mM), and glucose dehydrogenase (GDH; 10 U). PETN reductase reactions (1 mL) were performed anaerobically in buffer (50 mM KH_2PO_4/K_2HPO_4, pH 7.0) containing alkene (5 mM), PETNR (2 μM), $NADP^+$ (10 μM), glucose (15 mM), and glucose dehydrogenase (GDH; 10 U). All reactions were agitated at 30 °C for 4 or 24 h at 130 rpm. The alkenes were added from stock solutions in ethanol (2% final solvent concentration in the reactions). [b]Conversion (conv), yields, and cis/trans percentage were determined by GC analysis on a DB-WAX column.

stereospecificity could be achieved for the reduction of (R)-**12a** with recombinant NtDBR by the addition of bovine serum albumin (BSA). In addition, the presence of Triton X-100, γ-cyclodextrin, and casein were shown to improve the overall conversion.[13] Accordingly, we repeated the NtDBR-catalyzed reduction of (R)-**12a** in the presence of Triton X-100 ± BSA and in the presence of BSA alone. However, under our conditions, no improvement in conversion or stereospecificity was observed (results not shown). This may be due to differences in the sequence or folding of the two protein preparations. The originally published data[13] were obtained from protein expressed as a GST fusion, with the majority of the tag removed by proteolysis. In contrast, our data were obtained from C-terminally His$_6$-tagged protein. It is possible that the presence of different types of protein tags during protein expression has affected the conformation of the protein, leading to the observed differences in rate, stereospecificity, or both.

Interestingly, NtDBR-catalyzed reduction of (R)- and (S)-perillaldehyde (**13a**) generated the same major product from both enantiomers, cis-dihydroperillaldehyde (**13b**) (Table 5). This is not consistent with the net trans-hydrogenation mechanism observed for OYE-catalyzed alkene reduction, which is known to proceed via hydride transfer (from reduced flavin, FMNH$_2$) to the Cβ atom of the substrate and proton transfer (from a conserved tyrosine residue or water) to the Cα position of the substrate.[3] Indeed, control experiments with PETN reductase reflected net trans-hydrogenation, regardless of the substrate's absolute configuration, yielding trans-dihydroperillaldehyde and cis-dihydroperillaldehyde from (S)- and (R)-**13a**, respectively (Table 5). This unusual behavior has previously been observed for another member of the LTD subfamily, leukotriene B$_4$ 12-hydroxydehydrogenase (Ltb4dh), and was subsequently shown to originate from a divergent stereochemical pathway with (R)-perillaldehyde undergoing net trans-addition of H$_2$, whereas the reduction of (S)-perillaldehyde proceeded with net syn-addition of H$_2$.[29] This was reported as the first observation of its kind by a single enzyme. However, these results suggest it is highly likely that NtDBR and potentially other members of the LTD family share this unusual feature.

■ CONCLUSIONS

We have extended our study of "-ene" reductases to include NtDBR, a member of the LTD subfamily of the MDR enzymes. Substrate profiling, via steady-state kinetics and product identification techniques, has demonstrated its regio- and stereospecificity against a variety of α,β-unsaturated activated alkenes. In addition to high activity toward typical LTD substrates, NtDBR also catalyzed the reduction of several classical OYE-like substrates. Significantly, NtDBR also demonstrated activity toward non-OYE substrates (i.e., reducing the exocyclic C=C double bond of (R)-pulegone) as well as displaying the opposite enantioselectivity during the reduction of substrates such as (E)-2-phenyl-1-nitroprop-1-ene (**10a**) and (S)-perillaldehyde (**13a**) in comparison with the OYE family member PETN reductase. This complementary activity emphasizes the potential value of NtDBR as an industrial biocatalyst, in addition to classical OYE "-ene" reductases. Unlike OYE's, NtDBR also benefits from the absence of a bound flavin cofactor. Flavins can be oxidized by molecular oxygen at the expense of alkene reduction.[30] This results in an overall reduction in reaction rate and generates the reactive oxygen species (ROS) hydrogen peroxide and superoxide,[19a,30] the presence of which has been shown to sometimes influence product enantiopurity.[31]

We have also presented the X-ray crystal structures of the holo-, binary (NADP(H)-bound), and ternary [NADP$^+$ and 4-hydroxy-3-methoxycinnamaldehyde (**9a**)-bound] NtDBR complexes. The use of high-resolution structural information for the identification of individual residues/interactions, important in substrate binding and catalysis, is crucial for the generation of new biocatalysts with improved characteristics. Previously, we have achieved notable success in redefining the reactivities, stereochemistries, and specificities of the OYE family member PETN reductase using a robotic high-throughput kinetic screening of enzyme mutant libraries.[20,32] Although the ternary complex here shows the substrate bound in a conformation that is likely to be inhibitory, the position of HMHCA still provides information to aid the determination of which residues are likely to be involved in forming the alkene substrate binding pocket.

Structural and specificity data will be used to drive future structure-driven high-throughput site-saturated mutagenesis studies to further expand the biocatalytic potential of this

enzyme. Residues to be targeted include those that line the substrate binding pocket, although key conserved NAD(P)H-binding residues will be avoided. Residues further afield, such as ones involved in the overall protein fold and stability, may be targeted to allow larger substrates to be accommodated in the active site. In silico substrate binding studies could also drive site-directed mutagenesis studies, which may allow the likely role(s) of specific residues to be determined.

■ ASSOCIATED CONTENT

ⓢ Supporting Information

Discussion of additional details of the 3D X-ray crystal structures of DBR. This material is available free of charge via the Internet at http://pubs.acs.org.

■ AUTHOR INFORMATION

Corresponding Author

*Phone: +44 161 3065152. Fax: +44 161 3068918. E-mail: nigel.scrutton@manchester.ac.uk.

Author Contributions

§These authors contributed equally.

Notes

The authors declare no competing financial interest.

■ ACKNOWLEDGMENTS

■ REFERENCES

(1) (a) Nestl, B. M.; Nebel, B. A.; Hauer, B. *Curr. Opin. Chem. Biol.* **2011**, *15*, 187–193. (b) Panke, S.; Held, M.; Wubbolts, M. *Curr. Opin. Biotechnol.* **2004**, *15*, 272–279. (c) Schoemaker, H. E.; Mink, D.; Wubbolts, M. G. *Science* **2003**, *299*, 1694–1697. (d) Straathof, A. J. J.; Panke, S.; Schmid, A. *Curr. Opin. Biotechnol.* **2002**, *13*, 548–556.

(2) Turner, N. J. *Trends Biotechnol.* **2003**, *21*, 474–478.

(3) Stuermer, R.; Hauer, B.; Hall, M.; Faber, K. *Curr. Opin. Chem. Biol.* **2007**, *11*, 203–213.

(4) Toogood, H. S.; Gardiner, J. M.; Scrutton, N. S. *ChemCatChem* **2010**, *2*, 892–914.

(5) Nordling, E.; Jörnvall, H.; Persson, B. *Eur. J. Biochem.* **2002**, *269*, 4267–76.

(6) Youn, B.; Kim, S.-J.; Moinuddin, S. G. A.; Lee, C.; Bedgar, D. L.; Harper, A. R.; Davin, L. B.; Lewis, N. G.; Kang, C. *J. Biol. Chem.* **2006**, *281*, 40076–40088.

(7) Kasahara, H.; Jiao, Y.; Bedgar, D. L.; Kim, S.-J.; Patten, A. M.; Xia, Z.-Q.; Davin, L. B.; Lewis, N. G. *Phytochemistry* **2006**, *67*, 1765–1780.

(8) Dick, R. A.; Kwak, M. K.; Sutter, T. R.; Kensler, T. W. *J. Biol. Chem.* **2001**, *276*, 40803–40810.

(9) Matsushima, A.; Sato, Y.; Otsuka, M.; Watanabe, T.; Yamamoto, H.; Hirata, T. *Bioorg. Chem.* **2008**, *36*, 23–28.

(10) Zhang, Y.; Teoh, K. H.; Reed, D. W.; Covello, P. S. *Botany* **2009**, *87*, 643–649.

(11) Ringer, K. L.; McConkey, M. E.; Davis, E. M.; Rushing, G. W.; Croteau, R. *Arch. Biochem. Biophys.* **2003**, *418*, 80–92.

(12) Hirata, T.; Tamura, Y.; Yokobatake, N.; Shimoda, K.; Ashida, Y. *Phytochemistry* **2000**, *55*, 297–303.

(13) Hirata, T.; Matsushima, A.; Sato, Y.; Iwasaki, T.; Nomura, H.; Watanabe, T.; Toyoda, S.; Izumi, S. *J. Mol. Catal. B: Enzym.* **2009**, *59*, 158–162.

(14) Peterson, G. L. *Methods Enzymol.* **1983**, *91*, 95–119.

(15) Leslie, A. G. W. Recent changes to the MOSFLM package for processing film and image plate data. *Joint CCP4 & ESRF-EACBM Newsletter on Protein Crystallography*; 1992, 26

(16) Collaborative Computational Project Number 4. *Acta Crystallogr., Sect. D: Biol. Crystallogr.* **1994**, *50*, 760–763.

(17) Perrakis, A.; Morris, R.; Lamzin, V. S. *Nat. Struct. Biol.* **1999**, *6*, 458–63.

(18) Krissinel, E.; Henrick, K. *J. Mol. Biol.* **2007**, *372*, 774–797.

(19) (a) Fryszkowska, A.; Toogood, H.; Sakuma, M.; Gardiner, J. M.; Stephens, G. M.; Scrutton, N. S. *Adv. Synth. Catal.* **2009**, *351*, 2976–2990. (b) Toogood, H. S.; Fryszkowska, A.; Hare, V.; Fisher, K.; Roujeinikova, A.; Leys, D.; Gardiner, J. M.; Stephens, G. M.; Scrutton, N. S. *Adv. Synth. Catal.* **2008**, *350*, 2789–2803.

(20) Hulley, M. E.; Toogood, H. S.; Fryszkowska, A.; Mansell, D.; Stephens, G. M.; Gardiner, J. M.; Scrutton, N. S. *ChemBioChem* **2010**, *11*, 2433–2447.

(21) Dick, R. A.; Kensler, T. W. *J. Biol. Chem.* **2004**, *279*, 17269–77.

(22) Mano, J.; Torii, Y.; Hayashi, S.; Takimoto, K.; Matsui, K.; Nakamura, K.; Inze, D.; Babiychuk, E.; Kushnir, S.; Asada, K. *Plant Cell Physiol.* **2002**, *43*, 1445–1455.

(23) Adalbjornsson, B. V.; Toogood, H. S.; Fryszkowska, A.; Pudney, C. R.; Jowitt, T.; Leys, D.; Scrutton, N. S. *ChemBioChem* **2010**, *11*, 197–207.

(24) Persson, B.; Hedlund, J.; Jornvall, H. *Cell. Mol. Life Sci.* **2008**, *65*, 3879–3894.

(25) Holm, L.; Park, J. *Bioinformatics* **2000**, *16*, 566–567.

(26) Ohta, H.; Kobayashi, N.; Ozaki, K. *J. Org. Chem.* **1989**, *54*, 1802–1804.

(27) Fryszkowska, A.; Fisher, K.; Gardiner, J. M.; Stephens, G. M. *J. Org. Chem.* **2008**, *73*, 4295–4298.

(28) Shimoda, K.; Izumi, S.; Hirata, T. *Bull. Chem. Soc. Jpn.* **2002**, *75*, 813–816.

(29) Bougioukou, D. J.; Stewart, J. D. *J. Am. Chem. Soc.* **2008**, *130*, 7655–7658.

(30) Williams, R. E.; Bruce, N. C. *Microbiology* **2002**, *148*, 1607–1614.

(31) Fryszkowska, A.; Toogood, H. S.; Mansell, D.; Stephens, G.; Gardiner, J. M.; Scrutton, N. S. *FEBS J.* **2012**, *279*, 4160–4171.

(32) (a) Fryszkowska, A.; Toogood, H.; Sakuma, M.; Stephens, G. M.; Gardiner, J. M.; Scrutton, N. S. *Catal. Sci. Technol.* **2011**, *1*, 948–957. (b) Toogood, H. S.; Fryszkowska, A.; Hulley, M.; Sakuma, M.; Mansell, D.; Stephens, G. M.; Gardiner, J. M.; Scrutton, N. S. *ChemBioChem* **2011**, *12*, 738–749.